IEEE Access®
Multidisciplinary : Rapid Review : Open Access Journal

Load-aware operation strategy for wind turbines participating in the joint day-ahead energy and reserve market

NARENDER SINGH[1,2] (ID)**, SEYYED AHMAD HOSSEINI[3]** (ID)**,(Member, IEEE), JEROEN D. M. DE KOONING[1,2]** (ID)**,(Senior Member, IEEE), FRANÇOIS VALLÉE [3]** (ID)**,(Member, IEEE) and LIEVEN VANDEVELDE [1,2]** (ID)**, (Senior Member, IEEE)**

[1]Department of Electromechanical, Systems & Metal Engineering, Faculty of Engineering & Architecture, Ghent University, Tech Lane Ghent Science Park - Campus Ardoyen, Technologiepark-Zwijnaarde 131, B-9052 Ghent, Belgium
[2]FlandersMake@UGent - Corelab MIRO, Flanders Make, Belgium
[3]Electrical Power Engineering Unit (EPEU), Power Systems & Market Research Group, University of Mons, 7000 Mons, Belgium

Corresponding author: Narender Singh (e-mail: narender.singh@ugent.be).

ABSTRACT Wind power has emerged as a clean alternative to traditional power production, with a significant increase in its installed capacity observed over the past decade. In numerous regions, wind power producers are now afforded the opportunity to participate in day-ahead energy and reserve markets. In this context, the wind turbines can provide ancillary services such as frequency containment reserve (FCR). However, the provision of ancillary services is known to affect the physical loading on a wind turbine. This loading on different parts of the wind turbine can possibly result in sub-optimal performance leading to a reduced net power output or even a faster degradation of the wind turbine. On the other hand, no or low participation of a wind turbine in ancillary services market will lead to a lesser revenue on a long term. Moreover, low participation of wind turbines in the ancillary market will eventually limit the amount of wind power, since the ancillary services are needed to stabilise the grid and must then be provided by other energy sources. Addressing this challenge requires a holistic method to gauge both load and revenue for wind power producers (WPP), thus enabling them to make informed decisions. This study firstly presents a method of calculating major loads on the wind turbine. Then, a load-aware optimisation method of wind power scheduling in the joint day-ahead energy and reserve market (JERM) is proposed that provides WPPs, an ability to strike a balance between revenue and the physical loading of wind turbine.

INDEX TERMS Ancillary services, Frequency containment reserve, Wind turbines, Wind turbine loading, Wind turbine operation strategy

I. INTRODUCTION

IN 2022, 77.6 GW of new wind power installations were added globally. This sizeable increment brought the global installed wind energy capacity to 906.2 GW. The record installations from European nations, Sweden, Finland and Poland brought the total installed wind capacity in Europe in 2022 to 255.5 GW [1]. According to the International Energy Agency, the aim to achieve 61 % of total electricity generation from renewable energy by 2030 will only be possible with a threefold increase in renewable energy installations. The biggest contribution will be from wind and solar energy [2]. The net zero emissions by 2050 scenario requires a wind power generation of 7400 TWh per year by 2030 [3]. Only the future holds the answer to whether such monumental increase in renewable, and especially in wind power will be achieved.

Nevertheless, a significant growth is inevitable and necessary. The energy markets around the world are being reshaped due to the escalating share of wind energy in the global power mix. The reserve market landscape is also evolving due to these changes, as grid codes now allow wind power producer's (WPP) to participate in the provision of ancillary services [4].

As a result, extensive studies have been conducted within this domain. The possibility of temporary power over-production in variable speed wind turbines is explored in [5]. In [6], an active control of wind turbine for ancillary services using pitch and torque control methods is explored. The study presented in [7], presents a wind turbine participation in ancillary services market by the means of rotational kinetic energy. A grid frequency stabilisation strategy using inertial control of the wind turbine incorporating energy storage systems is

presented in [8]. The present studies are not only confined to frequency support service. In [9], a method of voltage control from a power plant is presented. The capability of wind farms to provide reactive power ancillary services is explained in [10] and [11]. Another study presented in [12] explores the coordination strategy of large wind farms for voltage support by the means of high converter capacity. An ancillary services provision method by the means of coordination between wind turbine and electrolysis systems is presented in [13]. The evolution of fast acting control systems for wind turbines has enabled the integration of wind farms into the ancillary services market [14]. In [15], a control system is presented that is capable of following the grid frequency with minimal error. An advanced converter control maintaining a transient frequency stability is presented in [16]. The study presented in [17], proposes a coordinated control strategy to efficiently utilise energy in permanent magnet synchronous generators (PMSG). A hybrid control strategy of frequency based power point tracking method is presented in [18]. In [19] control system capability for frequency containment reserve (FCR) and fast frequency response (FFR) is shown. A strategy incorporating wake control for optimised operation of wind farms providing FCR is proposed in [20]. These control techniques have made it possible for the wind turbines to have a deeper integration in ancillary services market. Crucial grid frequency services such as FCR and FFR can greatly benefit from these enhanced control capabilities of the wind turbines to swiftly respond to the grid frequency fluctuations. Grid services essential to maintain the grid stability such as synchronous inertial response, enhanced frequency response and fast post-fault active power recovery can also benefit from increased wind energy participation in the ancillary services market [21].

Studies point to an increase in the revenue of WPPs as a result of participating in the ancillary service market. A study exploring the advanced bidding strategy dedicated to optimal dispatch of WPP in the JERM is presented in [22]. The revenue generated using this technique has shown an increase in the revenue of WPP. A data-driven probabilistic energy and reserve bidding approach for wind turbines participating in reserve market has also concluded similar results [23].

Although the ancillary services market is a lucrative avenue for the WPPs, the physical loading of the wind turbine may be affected by these control techniques. There has been some research regarding the physical loading of the wind turbine. The impact of loads on composite wind turbine blades is studied in [24]. Loads on wind turbine blades are studied by using finite element analysis in [25]. Load identification of a wind turbine tower using Kalman filtering techniques is presented in [26]. Dynamic analysis of offshore wind turbine tower subjected to wind and wave loading is shown in [27]. There are also studies that explore the global physical loading of the wind turbine [28], [29] and [30]. Amidst all these studies, there exists limited literature on the effect of ancillary services provision on the loading of the wind turbine components. In [31], a study about the dynamic frequency control

considering wind turbine fatigue is presented. The effects of power reserve control on the structural loading of wind turbines are discussed in [32]. A control design to reduce the drive-train, blades and tower mechanical stresses of a wind turbine participating in the grid primary frequency regulation is presented in [33]. A non-linear virtual inertia control of wind turbines in order to enhance primary frequency response and suppressing drivetrain torsional oscillations is presented in [34]. A study presented in [35] studies the effect of primary reserve provision on the main bearing loads. These studies point to the different impacts of ancillary services provision on the wind turbine. However, none of the existing studies aims to combine these qualitatively to provide a metric for the overall loading of the wind turbine. Moreover, the economical aspect of the loading is not taken into account when considering the wind turbine participation in JERM. Hence, there is a need to quantify the overall major loads on a wind turbine, and moreover, to study the impact of ancillary service provision on these loads while integrating the techno-economic impact on the JERM participation.

To this end, this study proposes a load-aware optimisation method of wind power bidding in the JERM. The purpose of the developed method is not only to maximise the profit of the WPP but also to create an optimal balance between the net market revenue and the physical loads on the wind turbine. Firstly, a methodology is developed to calculate the physical loading on different components of the wind turbine, namely, the main bearing, the blades, the shaft and the tower. These loads are calculated for different reserve market bids. These loads are then used as an input into an optimisation problem that generates energy and reserve market bids for profit maximisation of the WPP while taking into account the wind turbine loading. This results in a load-aware operation strategy compromising economic profit with structural loading, which is the main novel contribution of this work.

This article is organised as follows: Section II describes the model and data used in this study. Section III presents the methodology used to calculate the loads on the wind turbine as well as the optimisation strategy. In Section IV, results from this study are discussed. The conclusion of this study is derived in Section V.

II. MODELS AND DATA

The models used in the study include the wind turbine, the PMSG and the control systems used for torque and pitch control of the wind turbine. Wind data is used to simulate these models for different cases. These models and data are detailed in this section.

A. WIND TURBINE AND WIND FIELD DESIGN

This study employs the NREL 5 MW offshore wind turbine model [36]. The model has been chosen for its high correspondence on the REpower 5M machine, which is a widely used wind turbine. The NREL 5 MW model is generally recognised and used as a benchmark in the field of wind energy. Its design and characteristics closely align with the

IEEE *Access*

TABLE 1. Wind turbine properties

Property	Specification
Power rating	5 MW
Nominal torque	4 MNm
Rotor orientation & configuration	Upwind, 3 blades
Rated rotor speed	12.1 rpm
Rotor and hub diameter	126 m and 3 m
Hub height	90 m
Cut-in, Rated and Cut-out wind speed	3 m/s, 11.4 m/s and 25 m/s

FIGURE 1. Power curve of a 5 MW wind turbine

real-world offshore wind turbines, offering a realistic representation for simulations and studies. The model incorporates design information gathered from various sources, including published documents from reputable turbine manufacturers. To develop and simulate the model, a wind turbine simulator called FAST v8 is used, which was developed by the National Renewable Energy Laboratory [37]. FAST v8 features several different modules including aerodynamics, structural loads, electrical system and hydrodynamic loads. To have a greater control on the control mechanism for this study, the electrical and pitch systems have been separately developed in Simulink. Moreover, the hydrodynamic loads module has not been included in this study as the focus of this study is on analysing the impact of dynamic control of the electric power on the turbine's structural loading. The primary characteristics of the wind turbine are listed in the Table 1.

The specified wind turbine operates in distinct regions, each of which is determined by the free-flow wind speed measured on the rotor of the turbine. These regions, depicted in Figure 1, are based on the wind speed at the turbine rotor. In Figure 1, Region 1 corresponds to wind speeds below 3 m/s, which is below the cut-in speed of the wind turbine. In this region, no torque is generated, and no power is extracted. In Region 2, the wind turbine functions in maximum power point tracking mode. Region 2.5 is the transition zone between Regions 2 and 3. Finally, in Region 3, the wind speeds exceed the nominal wind speed, and control methods limit the torque, speed, and power to prevent overloading of the drivetrain components. If the wind speed exceeds 25 m/s, the wind turbine enters the cut-out region, and no power is generated.

The wind data used for the simulations in this research work are generated by using TurbSim [38]. Two different cases have been simulated with the mean wind speed of 6 m/s and turbulence intensities of 5 % and 20 %, as presented in Figure 2 and Figure 3.

B. PERMANENT MAGNET SYNCHRONOUS GENERATOR

The study employs a PMSG. To accurately control the generator's performance, a rotating direct, quadrature (d,q) reference frame representation of the generator is used. Table 2 provides a comprehensive list of the generator parameters used in developing the model [39], [40]. It is worth noting that PMSGs have become increasingly popular in recent years due to their superior efficiency, high power density, and low maintenance requirements. Furthermore, modern wind turbines are increasingly using PMSGs, as they can operate
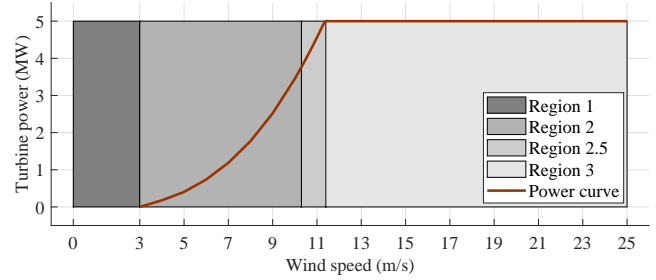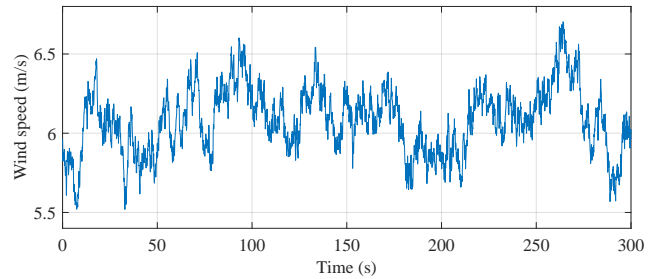

FIGURE 2. Wind profile with 5% turbulence intensity

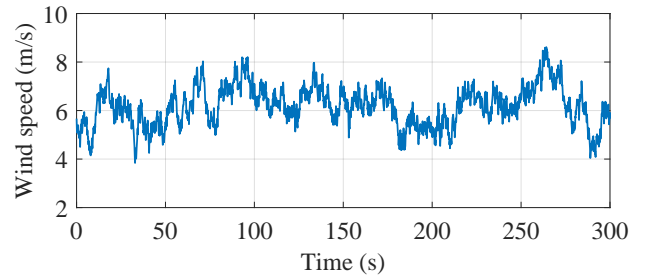**FIGURE 3. Wind profile with 20% turbulence intensity**

efficiently in variable speed conditions and allow direct-drive operation without gearbox.

C. CONTROL

The different control schemes used in the study are detailed in this section.

TABLE 2. Generator properties

Property	Specification
Rated power	5 MW
Rated speed	12.1 rpm
Nominal efficiency	93%
Pole pairs	117
Nominal voltage	1950 V
Nominal current	876 A
R_s, L_q	98.5 mΩ, 5.86 mH

1) Torque Control

The effectiveness of this study relies heavily on the accurate control of torque in the PMSG. To achieve this, Field Oriented Control (FOC) is employed in Simulink . In addition to FOC, other control strategies such as model predictive control and sliding mode control have been proposed for torque control in PMSG-based wind turbines [41]- [43]. However, FOC remains one of the most popular control strategies due to its simplicity and robustness [44], [45]. FOC regulates the quadrature current component $\hat{i}_q$ proportionally to the torque setpoint while keeping the direct current component $\hat{i}_d$ at zero for field orientation. The torque control scheme is depicted in Figure 4, with the Proportional Integral (PI) controller's proportional and integral gains set at 0.0001. All symbols represent the numerical values of the quantities in SI units. At each time step, the PI controller generates a current signal based on a comparison between the reference power $\hat{P}$ and actual power P. The current controller ensures that the desired current is generated to control the torque effectively. The reference power is determined by the grid frequency and the amount of contracted ancillary reserve. The Clarke-Park transformation is used to transform the three-phase abc current signals into the two-phase dq current components [46]. The resulting dq components are then used for torque control. The inverse Clarke-Park Transformation is subsequently applied to convert the dq components back to three-phase abc signals for modulation [47]. The PI controller is configured to minimise the tracking error by minimising overshoot and settling time. Although the controller's performance varies with changing wind speeds and the rate of change of the reference power, it is capable of tracking the reference power with minimal error. It is worth noting that accurate torque control is crucial for PMSGs to operate efficiently and deliver the desired power output.
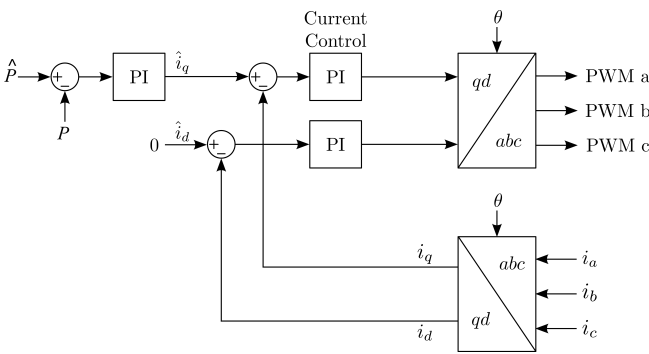

FIGURE 4. Field oriented control

2) Pitch Control

The Simulink-developed pitch control system is integrated with the wind turbine model in FAST to ensure smooth operation. During each iteration of the simulation, the pitch control system transmits a pitch command to each of the three blades of the wind turbine. Figure 5 illustrates the block diagram of the pitch control system, which employs a PI controller with proportional and integral gains of 206.3 and 25, respectively. The PI controller continuously compares the reference rotor speed, Ω_{ref}, a preset parameter, with the actual rotor speed, Ω, at each time step. The gain scheduling technique utilised a dimensionless gain correction factor, G, defined as in (1). The pitch angle, θ, plays a critical role in the gain scheduling process, and a tuning parameter, θ_d, is set to 0.055 radians to optimise its performance [48].

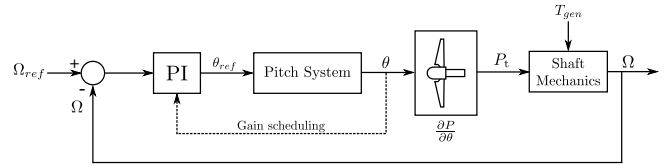$$G = \frac{1.6}{1 + \left(\frac{\theta}{2\theta_d}\right)} \tag{1}$$

FIGURE 5. Pitch control of the wind turbine blades

III. METHODOLOGY

The methodology used in this study is developed for a wind turbine participating in JERM, where bids are submitted day-ahead for energy and reserve markets by the WPP. The methodology is outlined in Figure 6. With the inputs of wind profile, grid frequency, model parameters and the reserve market bid, software-in-the-loop simulations are performed to calculate the loads on different sections of the wind turbine. As an output from these simulations a mapping between the reserve bid and total loading is achieved. Incorporating the derived loading map as a penalty term into the WPP's scheduling objective function, our proposed model strategically optimizes the WPP profit while mitigating wind turbine loads. The optimal decision variables of the model yield reserve and energy market bids. Additionally, the revenues and real-time compensations are also calculated. The following subsections present the calculation methods in detail.

A. LOAD CALCULATION

The total load on the wind turbine, referred to as L consists of 4 different loads. The *RMS* values of these loads from simulations for a time period of 300 s for each case are used. These loads associated with the main bearing, blades, shaft and the tower are presented in the following subsections.

1) Bearing load

The bearing load calculations are performed based on the method presented in [35]. The forces acting on the main bearing of the wind turbine are, axial force F_a (in N), lateral force F_v and vertical force F_l. Figure 7 shows these three forces acting on the wind turbine. F_a is calculated as the average of the 3 blade root forces F_{b1}, F_{b2} and F_{b3} as in (2). The radial force F_r (in N) is calculated using F_l and
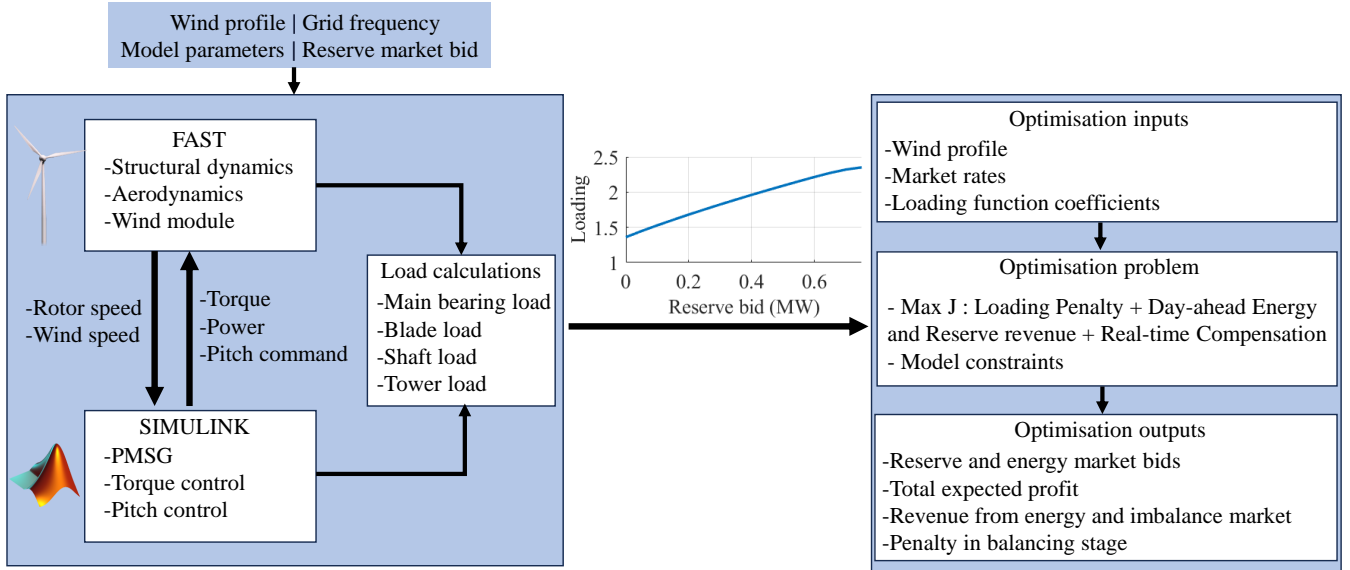
IEEE *Access*

FIGURE 6. Methodology

F_v as in (3). The root mean square (RMS) of the two forces are then used to calculate the dynamic equivalent force L_{br} acting on the main bearing as in (4). Here, t and T represent the time variable and the total duration of the simulation, respectively. b_x and b_y are dimensionless empirical factors for load calculations in a spherical roller bearing.

$$F_a = \frac{F_{b1} + F_{b2} + F_{b3}}{3} \qquad (2)$$

$$F_r = \sqrt{F_l^2 + F_v^2} \qquad (3)$$

$$L_{br} = \sqrt{\frac{1}{T} \int_0^T \left[b_x F_r(t) + b_y F_a(t) \right]^2 dt} \qquad (4)$$

2) Blade load

In the wind turbine model used for the simulations, each of the three blades are divided into 9 spans along the length of the blade. Each of these spans are subjected to forces directed along x, y and z axis. These forces and the division of the wind turbine blade in 9 spans is represented in Figure 7. The equivalent of the 3 forces on each span is calculated as per (5), where n is the number of blade (from 1 to 3) and m is the number of the span (from 1 to 9). The total blade load L_{bl} is then calculated as the RMS of the individual forces on each span of each blade as in (6). Note that the time dependence (t) is omitted to not overload the equations.

$$F_{bl_n,sp_m} = \sqrt{Fx_{bl_n,sp_m}^2 + Fy_{bl_n,sp_m}^2 + Fz_{bl_n,sp_m}^2} \qquad (5)$$
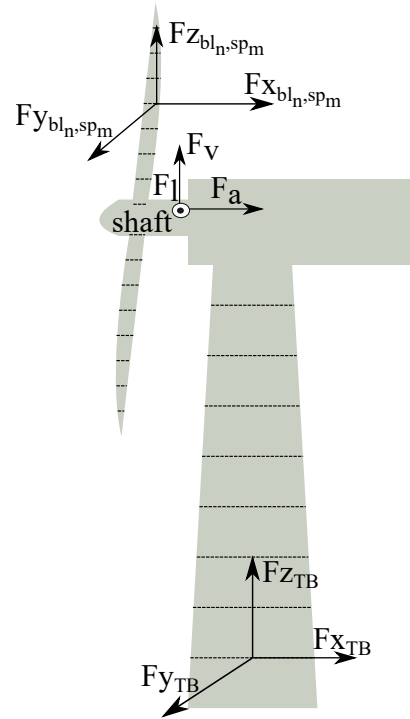

FIGURE 7. Forces acting on the wind turbine

$$L_{bl} = \sqrt{\frac{1}{T} \int_0^T \left(\sum_{m=1}^9 F_{bl_1,sp_m} + F_{bl_2,sp_m} + F_{bl_3,sp_m} \right)^2 dt} \qquad (6)$$

3) Shaft load

The shaft load comprises of rotating shaft bending moment at the shaft's strain gauge along y and z axis (in Nm). The bending moments are then divided by the distance from rotor apex to calculate the two equivalent forces Fy_{sh} and Fz_{sh} (in N) along y and z axis, respectively. These coordinates follow the similar plane as F_l and F_v, as shown in Figure 7. Finally, the total shaft load L_{sh} is calculated using the RMS of the equivalent forces as shown in (7).

$$L_{sh} = \sqrt{\frac{1}{T} \int_0^T \left[Fy_{sh}^2(t) + Fz_{sh}^2(t) \right] dt} \tag{7}$$

4) Tower load

The tower loads are divided into two categories, the loads associated with the main structure of the tower L_{TM} and the loads at the base of the tower L_{TB}. For the calculation of L_{TM}, the tower is divided into 9 sections. Each section of the tower is subjected to forces Fx_{TM}, Fy_{TM} and Fz_{TM} along x, y and z axis, respectively. The section of the wind turbine tower and associated forces are presented in Figure 7. The equivalent force at each of the sections is calculated as in (8), where k represents the section of the tower from 1 to 9. L_{TM} is then calculated as the sum of loads on each of the section as in (9). The tower base loads Fx_{TB}, Fx_{TB} and Fx_{TB} (in N) are directed along x, y and z axis respectively. The equivalent load on the tower base, L_{TB} is calculated as in (10). Finally, the total tower load L_{twr} is calculated as the sum of tower main and base loads as in (11).

$$L_{TM}(k) = \sqrt{Fx_{TM}^2(k) + Fy_{TM}^2(k) + Fz_{TM}^2(k)} \tag{8}$$

$$L_{TM} = \sqrt{\frac{1}{T} \int_0^T \left(\sum_{k=1}^{9} L_{TM}(k,t) \right)^2 dt} \tag{9}$$

$$L_{TB} = \sqrt{\frac{1}{T} \int_0^T \left[Fx_{TB}^2(t) + Fy_{TB}^2(t) + Fz_{TB}^2(t) \right] dt} \tag{10}$$

$$L_{twr} = L_{TM} + L_{TB} \tag{11}$$

5) Equivalent load

The total load on the wind turbine L is calculated as weighted sum the four individually calculated loads as in (12). Here, a, b, c and d are the weight factors associated with the loads. To determine the values of these weight factors, informed by their economic implications, a base case simulation is conducted over a duration of 3000 s. The weight factors based on the base case are setup such that each individual term on the right hand side of (12) is equivalent to 0.25. Hence, making the base value of L equal to 1. This arbitrary choice is made to demonstrate the functioning of the methodology. However, these are adjustable factors and can be tuned by the wind farm operator based on the economic costs associated with each of these components.

$$L = aL_{br} + bL_{bl} + cL_{sh} + dL_{twr} \tag{12}$$

B. OPTIMISATION

The optimisation strategy presented in [22] proposed a wind power scheduling framework that accounts for the revenue stream from both day ahead and real-time stages of the energy and reserve markets. However, in this strategy the loads acting on the wind turbine due to the optimal bids in JERM are not accounted for. For this study, the optimisation strategy has been improved to include the effect of wind turbine loading. The optimisation is performed in Matlab, using the Gurobi optimiser [49]. Based on the optimisation, optimal decisions are made to maximise the revenue of the WPP while taking the wind turbine physical loading into account. The objective function is stated in (13). Here, L as defined in (12) is the factor based on the mapping generated from the load calculations. The day-ahead bids related to the energy and reserve markets are, respectively, shown by Em_{bid} and Rm_{bid}. α is a dimensionless variable weight factor associated with the load L. λ_{sp} and λ_{cap} are the spot market and the reserve capacity prices, respectively. λ_{BU} and λ_{BD} are imbalance prices for surplus and deficit, respectively. λ_{cp} is the unavailability penalty price for the reserve. π_ω is the probability of occurrence of the scenario. δ_t is the market time unit equal to 1 hour. Ω/ω represents the scenario index/set. $\Delta P_{u\omega}$, $\Delta P_{d\omega}$ are the positive and negative deviation of injected power at scenario ω. $\Delta R_{d\omega}$ is the deviation of available capacity margin from the offered bid at scenario ω.

$$\begin{aligned} J = {} & -\alpha L + \lambda_{sp} Em_{bid} \Delta_t + \lambda_{cap} Rm_{bid} + \sum_{\omega \in \Omega} \\ & \pi_\omega \left\{ \Delta_t \left(\lambda_{BU} \Delta P_{u\omega} - \lambda_{BD} \Delta P_{d\omega} - \lambda_{cp} \Delta R_{d\omega} \right) \right\} \end{aligned} \tag{13}$$

The loading constraint used for the optimisation is shown in (14). This constraint takes into account the impact of increasing Rm_{bid} on the overall loading of the wind turbine. The choice of using only reserve market bid is based on the fact that the most influential factor of the wind turbine loading is the amount of reserve power provided since it has to be injected to the network dynamically thus affecting the load on the wind turbine. The values of p_1 and p_2 are calculated as shown in (15) and (16), where n refers to the number of data points simulated related to α.

$$L = p_1 Rm_{bid} + p_2 \tag{14}$$

$$p_1 = \frac{n \sum_{i=1}^{n} (Rm_{bid_i} L_i) - \left(\sum_{i=1}^{n} Rm_{bid_i} \right) \left(\sum_{i=1}^{n} L_i \right)}{n \sum_{i=1}^{n} Rm_{bid_i}^2 - \left(\sum_{i=1}^{n} Rm_{bid_i} \right)^2} \tag{15}$$

$$p_2 = \frac{\sum_{i=1}^{n} L_i - p_1 \sum_{i=1}^{n} Rm_{bid_i}}{n} \tag{16}$$

The other constraints associated with the optimisation are listed in (17)-(26). Here, Q_c is the amount of the offered bids

for the day-ahead market. P_ω, R_ω and Q_ω are the delivered power to the energy market, available reserve power and the total available wind power at scenario ω. M is a large positive constant for mixed integer programming. δ is the binary variable associated with the sufficient power capacity.

$$\text{Em}_{\text{bid}} + \text{Rm}_{\text{bid}} = \text{Q}_{\text{c}} \tag{17}$$

$$\text{P}_\omega + \text{R}_\omega = \text{Q}_\omega \tag{18}$$

$$\text{Em}_{\text{bid}} - \text{P}_\omega = \Delta P_{d\omega} - \Delta P_{u\omega} \tag{19}$$

$$\text{Rm}_{bid} - \text{R}_\omega \le \Delta R_{d\omega} \tag{20}$$

$$\text{Q}_\omega - \text{Rm}_{\text{bid}} - M\delta \le 0 \tag{21}$$

$$\text{Q}_\omega - \text{Rm}_{\text{bid}} + M(1-\delta) \ge 0 \tag{22}$$

$$\text{R}_\omega \le \text{Rm}_{\text{bid}} \tag{23}$$

$$\text{R}_\omega \le \text{Q}_\omega \tag{24}$$

$$\text{R}_\omega \ge \text{Rm}_{\text{bid}} - M(1-\delta) \tag{25}$$

$$\text{R}_\omega \ge \text{Q}_\omega - M\delta \tag{26}$$

C. REVENUE CALCULATION

The revenue calculations for a wind turbine participating in JERM are presented in this section. The total revenue consists of energy and reserve market revenues. All the revenue calculations are performed for a duration of 1 hour. The combined revenue from energy market and imbalance settlement, R_{EI} is calculated as shown in the (27). It accounts for the spot market price, the optimal reserve power bid, the positive and negative deviations of injected power and the respective imbalance prices for surplus and deficit.

$$R_{EI} = \lambda_{sp}\text{Em}_{\text{bid}}\Delta_t + \sum_{\omega \in \Omega} \pi_\omega \Delta_t (\lambda_{BU}\Delta P_{u\omega} - \lambda_{BD}\Delta P_{d\omega}) \tag{27}$$

The revenue generated by WPP in the day-ahead reserve market, R_{DR} is determined by multiplying the reserve capacity price by the optimal reserve power bid, as shown in (28).

$$R_{DR} = \lambda_{cap}\text{Rm}_{\text{bid}} \tag{28}$$

In (29), unavailability penalty price for the reserve and deviation of available capacity margin from the offered bid are used to calculate R_{PB}, the penalty incurred by WPP during the balancing stage.

$$R_{PB} = \sum_{\omega \in \Omega} \pi_\omega \Delta_t (-\lambda_{cp}\Delta R_{d\omega}) \tag{29}$$

The total revenue from participating in the reserve market and balancing stage, R_{RB}, as shown in (30), encompasses both the reserve capacity price and penalties. It takes into account the optimal reserve power bid, the unavailability penalty price, and the deviation of available capacity margin from the offered bid.

$$R_{RB} = \lambda_{cap}\text{Rm}_{\text{bid}} + \sum_{\omega \in \Omega} \pi_\omega \Delta_t (-\lambda_{cp}\Delta R_{d\omega}) \tag{30}$$

The overall profit R is the sum of various revenue components, including revenue from the energy market, reserve market, and imbalance settlement as shown in (31).

$$R = \lambda_{sp}\text{Em}_{\text{bid}}\Delta_t + \lambda_{cap}\text{Rm}_{\text{bid}} + \sum_{\omega \in \Omega}$$
$$\pi_\omega \Delta_t (\lambda_{BU}\Delta P_{u\omega} - \lambda_{BD}\Delta P_{d\omega} - \lambda_{cp}\Delta R_{d\omega}) \tag{31}$$

IV. RESULTS AND DISCUSSION

A first set of simulations is performed to find a mapping function between the reserve market bid and the loading of the wind turbine. The reserve bid is varied in the range of 0 MW to 0.75 MW in steps of 0.05 MW. These simulations are performed with a 6 m/s wind profile with 5 % and 20 % turbulence as shown in Section II-A. The other inputs to the coupled model of wind turbine and generator are, grid frequency, model parameters and the reserve market bid, as presented in Figure 6. For each of these simulations, the loads on different parts of the wind turbine are analysed. Figure 8 shows the forces in the base case which is simulated to define the base values of the weight factors associated with each of the 4 loads, as explained in Section III-A5. This simulation is performed for a duration of 3000 s. Figure 8 (a) and (b) show the axial and radial forces on the wind turbine bearing. Figure 8 (c) and (d) show the loads on the span 1 and span 9 of the blade. Figure 8 (e) and (f) show the load on shaft along the y and z axis. Figure 8 (g) and (h) show the main load and base load of the tower.

Table 3 and Table 4 present the results from the simulations in terms of the normalised loading for the cases of 5 % and 20 % wind turbulence intensity. Here, L_{br}, L_{bl}, L_{sh}, L_{twr} and L represent the bearing, blades, shaft, tower and the total loading respectively. The data in Table 3 and Table 4, while demonstrating a clear increasing trend in loading with respect to Rm_{bid}, also reveal a predominantly linear characteristic. This validates our decision to employ linear regression as detailed in Section III-B, through (14) - (16). As Rm_{bid} increases from 0 to 0.75 MW, there is a noticeable rise in each of the loading terms. For the 5 % turbulence case, L_{br} exhibits a consistent increasing progression with its value increasing from 0.471 for no reserve bid to 1.027 for the highest reserve bid in the range. For the case of 20 % turbulence, this rise is from 0.378 to 0.897. Similarly, L_{bl} shows a consistent increment from 0.403 to 0.828 for 5 % turbulence case and 0.335 to 0.726 for the 20 % turbulence case, as Rm_{bid} increases. In contrast, for the 5 % turbulence case, L_{sh} and L_{twr} demonstrate a relatively marginal increase from 0.236 to 0.246 and 0.25 to 0.251 across the same Rm_{bid} range, respectively. Notably, L_{sh} stabilises from Rm_{bid} value of 0.25 MW onwards. A similar trend is observed for the case of 20 % wind turbulence intensity. With the maximum influence coming from L_{br} and L_{bl}, L_{total} shows a consistent upward trend. The increased L is due to the increased control action that in turn effects the forces acting on different components of the wind turbine. This dataset establishes the relationship between Rm_{bid} and the corresponding load variations, indicating a trend of load

This article has been accepted for publication in IEEE Access. This is the author's version which has not been fully edited and content may change prior to final publication. Citation information: DOI 10.1109/ACCESS.2024.3350439

IEEE *Access*

Author *et al.*: Preparation of Papers for IEEE TRANSACTIONS and JOURNALS
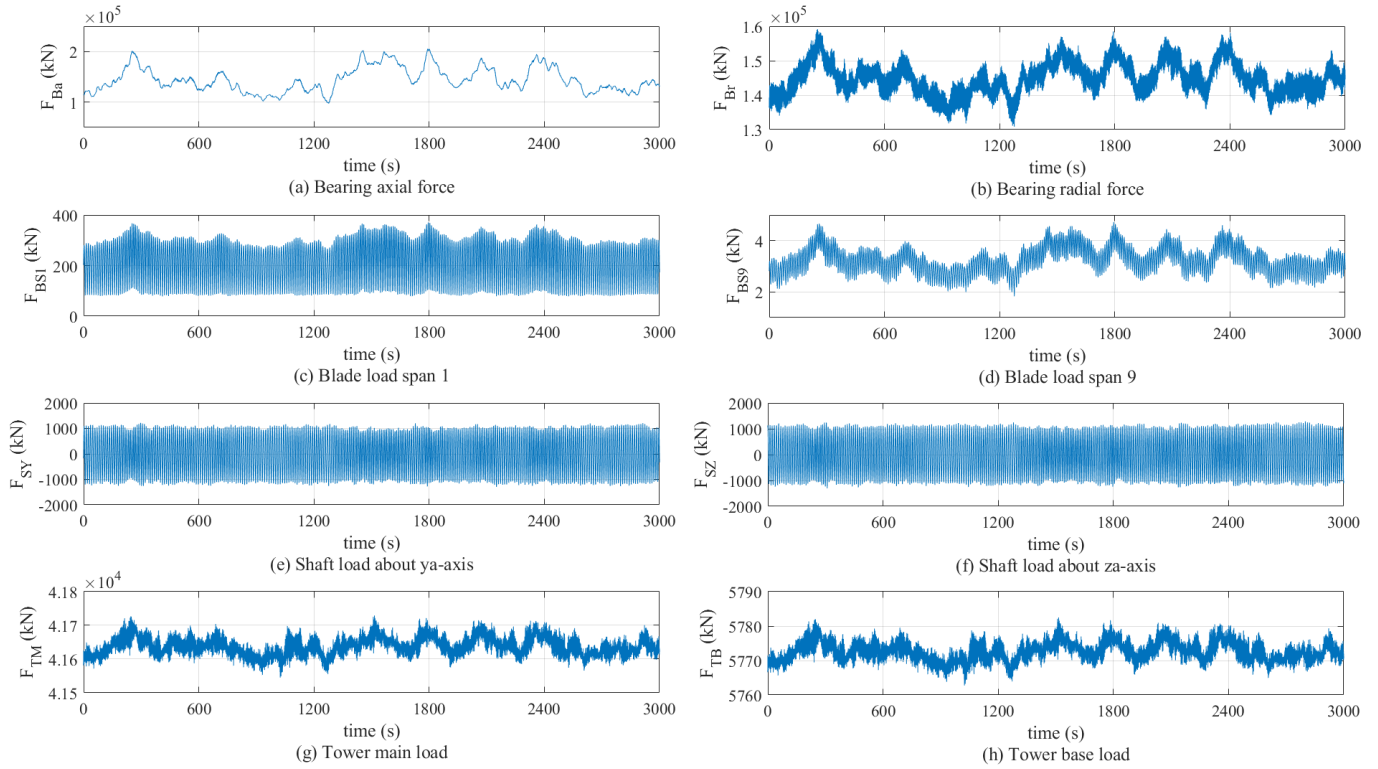
FIGURE 8. Forces acting of different wind turbine components

increases with the rise in $\mathrm{Rm_{bid}}$. A corresponding graph between the cumulative L and $\mathrm{Rm_{bid}}$ is shown in Figure 9.
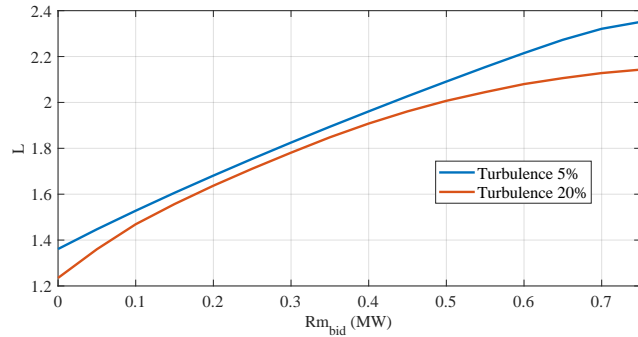

FIGURE 9. Reserve market bid versus Loading

The next set of simulations are performed by the optimisation model (13)-(26), to evaluate the optimal market bids in order to balance the wind turbine loads and the WPP's revenue. The values of λ_{sp}, λ_{cap}, λ_{BU}, λ_{BD} and λ_{cp} for revenue related calculations are € 33, € 34, € 30, € 35 and € 45, respectively. These market rates are in a similar and comparable range as in the related literature [22], [23] and several European electricity markets, such as in Denmark, Norway, and Belgium [50], [51]. In these simulations of a time period of 1 hour each, different scenarios are studied in terms of α, which is the weight factor associated with L. The

intent is to analyse the impact of weightage (α) of L on the revenue and the optimised bids. Table 5 and Table 6 present a synopsis of the reserve market bids and expected revenue from JERM for the two simulated cases of 5 % and 20 % wind turbulence intensity, respectively. An examination of the data shows the impact of changing α on the optimal bid and various presented revenues. Firstly, it is evident that $\mathrm{Rm_{bid}}$ decreases with the increasing α. For the 5 % turbulence case, the maximum reserve bid of 0.60 *MW* is offered when α is zero. This bid is the maximum possible reserve market bid, equivalent to a bid when the L is not taken into account for the optimisation. As the value of α gradually increases, a decreasing trend is observed in the $\mathrm{Rm_{bid}}$. Eventually, for α values 75 and higher, the corresponding $\mathrm{Rm_{bid}}$ is zero. For the case of 5 % turbulence intensity, the maximum $\mathrm{Rm_{bid}}$ of 0.28 MW is observed when α is zero. It can be noticed that, $\mathrm{Rm_{bid}}$ offered for the case of 20 % turbulence intensity is lower in comparison to th 5 % turbulence intensity case. This is due to the fact that with a higher level of turbulence in the wind, more fluctuations in the wind are present that eventually lead to more instances of lower wind speed. The optimisation algorithm developed for this study takes these uncertainties into account for the calculation of the optimal $\mathrm{Rm_{bid}}$.

The revenues associated with each scenario and the total profit are presented in Table 5 and Table 6. The revenue from energy market and imbalance settlements, R_{EI} shows proportionate changes to the values of α. For the 5 % turbulence case, the value of R_{EI} rises from € 5.02 to € 24.52, as α

Rm_{bid} / Loading	0	0.05	0.10	0.15	0.20	0.25	0.30	0.35	0.40	0.45	0.50	0.55	0.60	0.65	0.70	0.75
L_{br}	0.471	0.522	0.568	0.611	0.654	0.695	0.735	0.773	0.811	0.847	0.883	0.918	0.952	0.984	1.010	1.027
L_{bl}	0.403	0.440	0.474	0.507	0.539	0.570	0.601	0.630	0.659	0.687	0.715	0.742	0.769	0.794	0.815	0.828
L_{sh}	0.236	0.236	0.237	0.238	0.238	0.239	0.240	0.241	0.242	0.242	0.243	0.244	0.245	0.245	0.245	0.246
L_{twr}	0.250	0.250	0.250	0.250	0.250	0.251	0.251	0.251	0.251	0.251	0.251	0.251	0.251	0.251	0.251	0.251
L_{total}	1.361	1.447	1.528	1.606	1.681	1.754	1.825	1.894	1.961	2.027	2.091	2.154	2.215	2.273	2.321	2.351

TABLE 3. Normalised loading associated with the changing Rm_{bid} [MW], wind turbulence intensity 5 %

Rm_{bid} / Loading	0	0.05	0.10	0.15	0.20	0.25	0.30	0.35	0.40	0.45	0.50	0.55	0.60	0.65	0.70	0.75
L_{br}	0.378	0.457	0.520	0.570	0.615	0.656	0.696	0.733	0.766	0.796	0.821	0.843	0.862	0.876	0.889	0.897
L_{bl}	0.335	0.393	0.439	0.476	0.510	0.541	0.571	0.600	0.625	0.648	0.668	0.684	0.699	0.711	0.720	0.726
L_{sh}	0.260	0.260	0.260	0.261	0.262	0.263	0.264	0.265	0.266	0.267	0.267	0.268	0.268	0.269	0.269	0.269
L_{twr}	0.250	0.250	0.250	0.250	0.250	0.250	0.251	0.251	0.251	0.251	0.251	0.251	0.251	0.251	0.251	0.251
L_{total}	1.235	1.360	1.469	1.557	1.637	1.711	1.781	1.848	1.908	1.961	2.007	2.045	2.080	2.106	2.128	2.143

TABLE 4. Normalised loading associated with the changing Rm_{bid} [MW], wind turbulence intensity 20 %

increases up to 75. Whereas, for the case of 20 % turbulence, R_{EI} increases from € 18.63 to € 27.49. The growth indicates that the increasing values of α positively influence the revenue from the energy market. This is because with higher values of α, a greater portion of energy is designated for Em_{bid}, while a lower amount is set aside for Rm_{bid}. This occurs due to the negative term L in the objective function being directly influenced by Rm_{bid}. Expanding on this, it can be observed that for both the turbulence case, the revenue for the reserve market, R_{RB} is highest for the lower values of α and gradually decreases as the value of α increases. However, it should be noted that the R_{RB} is the less dominant mode of revenue for the case of 20 % turbulence as compared to the 5 % turbulence case. This is due to the optimisation algorithm that accounts for the reserve unavailability. R_{RB} is a combined sum of the revenue in the reserve market R_{DR} and the penalty in balancing stage R_{PB}. R_{DR} is bound with α and thereby by Rm_{bid}. Similar is the case for R_{PB}. As α grows, the amount of reserve offered reduces. As a result, due to the lower WPP's deviations from the planned capacities, lower penalties are incurred. The overall profit of the wind turbine participation in JERM, the total revenue, R is also presented in Table 5 and Table 6. The values of R include the revenues from energy and reserve markets along with the penalties due to the unavailability. It can be seen here that the maximum profit is earned when the value of α is zero, indicating that the impact of loading, L is not taken into account. The least revenue is observed for the higher values of α.

Another key observation is made by identifying the knee point in the data trend. This is achieved by calculating the difference between consecutive data points of Rm_{bid} and R. The allocated reserve bid Rm_{bid} and total revenue R, as presented in Table 5, pinpoint a knee point at the α value of 75, as illustrated in Figure 10 and Figure 11. This suggests that decision-makers can prioritize the loading of the wind turbine over a broad range without sacrificing profit, up to an α value of 75. However, if the emphasis on the wind turbine loading becomes significantly pronounced, the rate of change in revenue (or the potential for revenue loss) becomes steeper, rather than gradual. It should be noted that the values presented here are for a single wind turbine, for 1 hour and for a low wind speed scenario. The cumulative difference in the profit for a longer duration and for an entire farm can be highly significant in the interest of WPPs.

V. CONCLUSION

This study presents a novel method of wind turbine participation in JERM using a load-aware profit maximising approach. A methodology is developed to aggregate the major loads of the wind turbine and present it as a single unit. The loading factor generated from this methodology acknowledges the loads on the blade, main bearing, shaft and the tower of the wind turbine. The aggregate loading is then used as an input to the optimisation problem that, given the constraints, maximises the WPP's profit while minimising the physical loading of the wind turbine. The results of this study indicate

This article has been accepted for publication in IEEE Access. This is the author's version which has not been fully edited and content may change prior to final publication. Citation information: DOI 10.1109/ACCESS.2024.3350439

IEEE Access

Author *et al.*: Preparation of Papers for IEEE TRANSACTIONS and JOURNALS

α	Rm_{bid} [MW]	R_{EI} [€]	R_{RB} [€]	R_{DR} [€]	R_{PB} [€]	R [€]
0	0.60	5.02	20.04	20.29	-0.25	25.06
5	0.59	5.15	19.91	20.15	-0.24	25.06
10	0.59	5.31	19.75	19.97	-0.22	25.06
15	0.58	5.47	19.59	19.78	-0.19	25.06
20	0.57	5.70	19.36	19.53	-0.17	25.06
25	0.57	5.83	19.23	19.38	-0.16	25.05
30	0.56	6.05	19.00	19.14	-0.14	25.05
35	0.56	6.26	18.79	18.91	-0.12	25.05
40	0.55	6.45	18.59	18.70	-0.10	25.05
45	0.54	6.73	18.31	18.40	-0.09	25.04
50	0.53	6.99	18.05	18.12	-0.08	25.04
55	0.52	7.53	17.50	17.55	-0.05	25.02
60	0.49	8.25	16.75	16.79	-0.03	25.01
65	0.46	9.19	15.79	15.81	-0.01	24.98
70	0.44	10.16	14.79	14.80	0.00	24.95
75	0.00	24.52	0.00	0.00	0.00	24.52
80	0.00	24.52	0.00	0.00	0.00	24.52

TABLE 5. Revenues as a function of α, wind turbulence intensity 5 %

α	Rm_{bid} [MW]	R_{EI} [€]	R_{RB} [€]	R_{DR} [€]	R_{PB} [€]	R [€]
0	0.28	18.63	9.01	9.63	-0.61	27.64
5	0.26	19.39	8.25	8.75	-0.50	27.64
10	0.25	19.68	7.96	8.42	-0.46	27.64
15	0.24	19.95	7.69	8.12	-0.43	27.64
20	0.22	20.38	7.25	7.63	-0.38	27.63
25	0.21	20.73	6.90	7.24	-0.34	27.63
30	0.18	21.61	6.02	6.28	-0.26	27.62
35	0.18	21.78	5.83	6.08	-0.25	27.62
40	0.14	22.98	4.62	4.78	-0.16	27.60
45	0.13	23.25	4.34	4.49	-0.15	27.59
50	0.12	23.69	3.89	4.02	-0.12	27.59
55	0.06	25.64	1.90	1.94	-0.04	27.54
60	0.04	26.35	1.18	1.20	-0.02	27.53
65	0.02	26.94	0.57	0.58	-0.01	27.51
70	0.00	27.41	0.09	0.09	0.00	27.50
75	0.00	27.49	0.00	0.00	0.00	27.49
80	0.00	27.49	0.00	0.00	0.00	27.49

TABLE 6. Revenues as a function of α, wind turbulence intensity 20 %

FIGURE 10. Variation in Rm_{bid} with respect to α

FIGURE 11. Variation in R with respect to α

and loss remains minimal across a broad range of loading weights before experiencing a significant drop with only a slight change in loading weight. Therefore, decision-makers should identify the knee point in their data, as demonstrated in this study, to ensure a profit that does not compromise turbine health significantly. The weight factors *a*, *b*, *c* and *d* associated with the loads as defined in the study, provide the WPP a useful tool at their disposal. These factors can be tuned as per the costs and condition of these wind turbine components. Additionally, the factor α associated with the physical loading in the bidding optimisation is an adjustable factor that can be tuned to balance the revenue and the loading as per the requirement of the WPP. In this way the WPPs always have a trade-off option to create a balance between the physical load on the wind turbine and the monetary benefit.

ACKNOWLEDGMENT

that the physical loading of the wind turbine can be effectively modeled as a function of the reserve bid. It is observed that when considering the wind turbine loading in wind power scheduling, a lower reserve bid is achieved as the loading weight increases. Similarly, as the loading weight rises, the market revenue decreases. This is because, unlike traditional scheduling models that overlook the wind turbine loading and its hidden costs, our model implicitly accounts for the costs associated with the wind turbine physical health. Another crucial consideration for decision-makers is that the profit
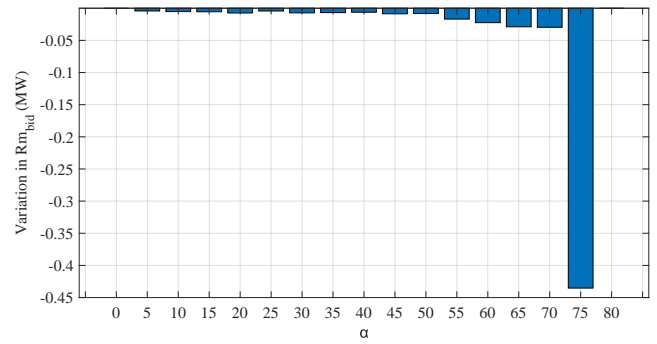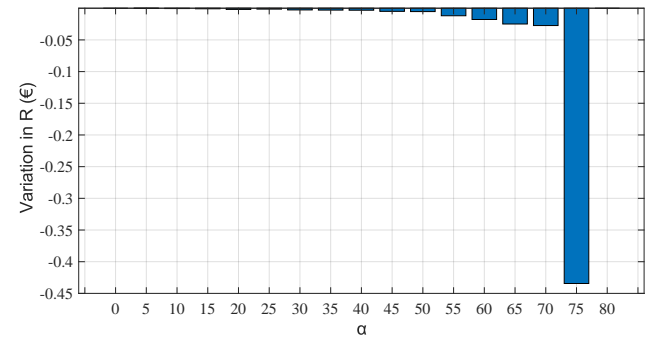
REFERENCES

[1] Global wind energy council, 2023. Global wind report. [online] Available at: https://gwec.net/globalwindreport2023/ [Accessed: 25- Apr- 2023].
[2] World energy outlook 2022. [online] Available at: https://www.iea.org/reports/world-energy-outlook-2022 [Accessed: 25- Apr- 2023].

IEEE *Access*

[3] IEA (2022), Wind Electricity, IEA, Paris https://www.iea.org/reports/wind-electricity, License: CC BY 4.0 [Accessed: 25- Apr- 2023].

[4] Technical Requirements for the Connection of Generating Stations to the Hydro-Québec Transmission System. 2019. Available online: http://www.hydroquebec.com/ (accessed on 1 September 2022)

[5] G. C. Tarnowski, P. C. Kjær, P. E. Sørensen and J. Østergaard, "Variable speed wind turbines capability for temporary over-production," 2009 IEEE Power & Energy Society General Meeting, Calgary, AB, Canada, 2009, doi: 10.1109/PES.2009.5275387.

[6] J. Aho, P. Fleming and L. Y. Pao, "Active power control of wind turbines for ancillary services: A comparison of pitch and torque control methodologies," 2016 American Control Conference (ACC), Boston, MA, USA, 2016, pp. 1407-1412, doi: 10.1109/ACC.2016.7525114.

[7] A. Žertek, G. Verbič and M. Pantoš, "Participation of DFIG wind turbines in frequency control ancillary service by optimized rotational kinetic energy," 2010 7th International Conference on the European Energy Market, Madrid, Spain, 2010, pp. 1-6, doi: 10.1109/EEM.2010.5558666.

[8] C. Nikolakakos, U. Mushtaq, P. Palensky and M. Cvetković, "Improving Frequency Stability with Inertial and Primary Frequency Response via DFIG Wind Turbines equipped with Energy Storage System," 2020 IEEE PES Innovative Smart Grid Technologies Europe (ISGT-Europe), The Hague, Netherlands, 2020, doi: 10.1109/ISGT-Europe47291.2020.9248807.

[9] H. Karbouj and Z. H. Rather, "Voltage Control Ancillary Service From Wind Power Plant," in IEEE Transactions on Sustainable Energy, vol. 10, no. 2, pp. 759-767, April 2019, doi: 10.1109/TSTE.2018.2846696.

[10] N. R. Ullah, K. Bhattacharya and T. Thiringer, "Wind Farms as Reactive Power Ancillary Service Providers—Technical and Economic Issues," in IEEE Transactions on Energy Conversion, vol. 24, no. 3, pp. 661-672, Sept. 2009, doi: 10.1109/TEC.2008.2008957.

[11] E. Gatavi, A. Hellany, M. Nagrial and J. Rizk, "An integrated reactive power control strategy for improving low voltage ride-through capability," in Chinese Journal of Electrical Engineering, vol. 5, no. 4, pp. 1-14, Dec. 2019, doi: 10.23919/CJEE.2019.000022.

[12] Z. Dong, Z. Li, L. Du, Y. Liu and Z. Ding, "Coordination Strategy of Large-Scale DFIG-Based Wind Farm for Voltage Support With High Converter Capacity Utilization," in IEEE Transactions on Sustainable Energy, vol. 12, no. 2, pp. 1416-1425, April 2021, doi: 10.1109/TSTE.2020.3047273.

[13] X. Cheng et al., "A Coordinated Frequency Regulation and Bidding Method for Wind-Electrolysis Joint Systems Participating Within Ancillary Services Markets," in IEEE Transactions on Sustainable Energy, vol. 14, no. 3, pp. 1370-1384, July 2023, doi: 10.1109/TSTE.2022.3233062.

[14] S. A. Hosseini et Al., "Impact Of Fast Wind Fluctuations On The Profit Of A Wind Power Producer Jointly Trading In Energy And Reserve Markets," The 9th Renewable Power Generation Conference (Rpg Dublin Online 2021), Online Conference, 2021, Pp. 240-245, Doi: 10.1049/Icp.2021.1386.

[15] N. Singh, J. D. M. De Kooning and L. Vandevelde, "Simulation of the Primary Frequency Control Pre-Qualification Test for a 5MW Wind Turbine," 2020 IEEE/PES Transmission and Distribution Conference and Exposition (T&D), Chicago, IL, USA, 2020, doi: 10.1109/TD39804.2020.9299921.

[16] J. Daković, P. Ilak, T. Baškarad, M. Krpan and I. Kuzle, "Effectiveness of wind turbine fast frequency response control on electrically distanced active power disturbance mitigation," Mediterranean Conference on Power Generation, Transmission, Distribution and Energy Conversion (MED-POWER 2018), Dubrovnik, Croatia, 2018, doi: 10.1049/cp.2018.1923.

[17] H. Kim, J. Lee, J. Lee, and G. Jang, "Novel Coordinated Control Strategy of BESS and PMSG-WTG for Fast Frequency Response," Applied Sciences, vol. 11, no. 9, Apr. 2021, doi: 10.3390/app11093874.

[18] X. Zhao, Z. Lin and B. Fu, S. Gong, "Research on frequency control method for micro-grid with a hybrid approach of FFR-OPPT and pitch angle of wind turbine", International Journal of Electrical Power & Energy Systems, 2021, doi:10.1016/j.ijepes.2020.106670.

[19] N. Singh, J.D.M.De Kooning and L. Vandevelde: Dynamic wake analysis of a wind turbine providing frequency support services. IET Renewable Power Generation 16, 1853–1865 (2022). doi:10.1049/rpg2.12455

[20] N. Kayedpour, J. D. M. De Kooning, A. E. Samani, F. Kayedpour, L. Vandevelde and G. Crevecoeur, "An Optimal Wind Farm Operation Strategy for the Provision of Frequency Containment Reserve Incorporating Active Wake Control," in IEEE Transactions on Sustainable Energy, doi: 10.1109/TSTE.2023.3288130.

[21] Energy Storage Applications Summary, 2020. European Association for Storage of Energy. [online] Available at: https://ease-storage.eu/wp-content/uploads/2020/06/ES-Applications-Summary.pdf [Accessed 6 May 2022]

[22] S. A. Hosseini, J. F. Toubeau, Z. De Grève and F. Vallée, "An advanced day-ahead bidding strategy for wind power producers considering confidence level on the real-time reserve provision", Volume 280, 2020, 115973, ISSN 0306-2619, Applied Energy, doi:10.1016/j.apenergy.2020.115973.

[23] S. A. Hosseini, J. -F. Toubeau, N. Amjady and F. Vallée, "Day-Ahead Wind Power Temporal Distribution Forecasting With High Resolution," in IEEE Transactions on Power Systems, doi: 10.1109/TPWRS.2023.3295915.

[24] A. S. Verma, J. Y., W. Hu, Z. Jiang, W. Shi and J.J.E. Teuwen, "A review of impact loads on composite wind turbine blades: Impact threats and classification", Renewable and Sustainable Energy Reviews, 2023, doi:10.1016/j.rser.2023.113261.

[25] R. P. Tavares, V. Bouwman and W. Van Paepegem, "Finite element analysis of wind turbine blades subjected to torsional loads: Shell vs solid elements", Composite Structures, 2022, doi:10.1016/j.compstruct.2021.114905.

[26] D. Wei, D. Li, T. Jiang, P. Lyu, X. Song, Load identification of a 2.5 MW wind turbine tower using Kalman filtering techniques and BDS data, Engineering Structures, 2023, https://doi.org/10.1016/j.engstruct.2023.115763.

[27] Y. Hu, J. Yang, C. Baniotopoulos, X. Wang and X. Deng, "Dynamic analysis of offshore steel wind turbine towers subjected to wind, wave and current loading during construction", Ocean Engineering, 2020, doi:10.1016/j.oceaneng.2020.108084.

[28] S. Wang, T. Moan and Z. Gao, "Methodology for global structural load effect analysis of the semi-submersible hull of floating wind turbines under still water, wind, and wave loads", Marine Structures, 2023, doi:10.1016/j.marstruc.2023.103463.

[29] S. Wang, Y. Xing, R. Balakrishna, W. Shi and X. Xu, "Design, local structural stress, and global dynamic response analysis of a steel semi-submersible hull for a 10-MW floating wind turbine", Engineering Structures, 2023, doi:10.1016/j.engstruct.2023.116474.

[30] N. Beganovic, J. Njiri, and D. Söffker, "Reduction of Structural Loads in Wind Turbines Based on an Adapted Control Strategy Concerning Online Fatigue Damage Evaluation Models," Energies, vol. 11, no. 12, p. 3429, Dec. 2018, doi: 10.3390/en11123429.

[31] X. Wang, Y. Wang, and Y. Liu, (2020). "Dynamic load frequency control for high-penetration wind power considering wind turbine fatigue load". International Journal of Electrical Power & Energy Systems, 117, 105696. doi: 10.1016/j.ijepes.2019.105696

[32] P. A. Fleming, J. Aho, A. Buckspan, E. Ela, Y. Zhang, V. Gevorgian, A. Scholbrock, L. Pao, and R. Damiani. (2016) "Effects of power reserve control on wind turbine structural loading" in Wind Energy, 19: 453–469. doi: 10.1002/we.1844.

[33] H. Camblong, I. Vechiu, A. Etxeberria, M.I. Martínez, "Wind turbine mechanical stresses reduction and contribution to frequency regulation", in Control Engineering Practice, Volume 30, 2014, doi:10.1016/j.conengprac.2014.03.007.

[34] B. Liu, J. Zhao, Q. Huang, F. Milano, Y. Zhang and W. Hu, "Nonlinear Virtual Inertia Control of WTGs for Enhancing Primary Frequency Response and Suppressing Drivetrain Torsional Oscillations," in IEEE Transactions on Power Systems, Sept. 2021, doi: 10.1109/TPWRS.2021.3055262.

[35] N. Singh, D. Boruah, J. D. M. De Kooning, W. De Waele, and L. Vandevelde, "Impact Assessment of Dynamic Loading Induced by the Provision of Frequency Containment Reserve on the Main Bearing Lifetime of a Wind Turbine," Energies, vol. 16, no. 6, p. 2851, Mar. 2023, doi: 10.3390/en16062851.

[36] J. Jonkman, S. Butterfield, W. Musial, and G. Scott. (2009). "Definition of a 5-MW Reference Wind Turbine for Offshore System Development." [online] Available at: https://www.nrel.gov/docs/fy09osti/38060.pdf

[37] J. Jonkman, (2016). FAST (Version V8) [Software]. NREL. https://www.nrel.gov/wind/nwtc/fastv8.html

[38] 'TubSim'. NREL. Available at: https://www.nrel.gov/wind/nwtc/turbsim.html.

[39] J. D. M. De Kooning, J. Van de Vyver, B. Meersman and L. Vandevelde, "Maximum efficiency current waveforms for a PMSM including iron losses and armature reaction," 2016 XXII International Conference on Electrical Machines (ICEM), Lausanne, Switzerland, 2016, doi: 10.1109/ICEL-MACH.2016.7732779.

[40] L. Sethuraman and K. L. Dykes, Generatorse: A sizing tool for variable-speed wind turbine generators, 2017. doi:10.2172/1395455

[41] M. E. Zarei, D. Ramírez, M. Prodanovic and G. M. Arana, "Model Predictive Control for PMSG-Based Wind Turbines With Overmodulation and Adjustable Dynamic Response Time," in IEEE Transactions on

Industrial Electronics, vol. 69, no. 2, pp. 1573-1585, Feb. 2022, doi: 10.1109/TIE.2021.3057021.

[42] A. -R. Youssef, E. E. M. Mohamed and A. I. M. Ali, "Model predictive control for grid-tie wind-energy conversion system based PMSG," 2018 International Conference on Innovative Trends in Computer Engineering (ITCE), Aswan, Egypt, 2018, pp. 467-472, doi: 10.1109/ITCE.2018.8316668.

[43] S. M. Mozayan, M. Saad, H. Vahedi, H. Fortin-Blanchette and M. Soltani, "Sliding Mode Control of PMSG Wind Turbine Based on Enhanced Exponential Reaching Law," in IEEE Transactions on Industrial Electronics, vol. 63, no. 10, pp. 6148-6159, Oct. 2016, doi: 10.1109/TIE.2016.2570718.

[44] C. Busca, A. -I. Stan, T. Stanciu and D. I. Stroe, "Control of Permanent Magnet Synchronous Generator for large wind turbines," 2010 IEEE International Symposium on Industrial Electronics, Bari, Italy, 2010, pp. 3871-3876, doi: 10.1109/ISIE.2010.5637628.

[45] H. Salime, B. Bossoufi, S. Motahhir, Y. E. Mourabit, A novel combined FFOC-DPC control for wind turbine based on the permanent magnet synchronous generator, Energy Reports, Volume 9, 2023, https://doi.org/10.1016/j.egyr.2023.02.012.

[46] R. H. Park, "Two-reaction theory of synchronous machines", AIEE Transactions, 1929.

[47] P. Krause, O. Wasynczuk, S. D. Sudhoff, and S. Pekarek. Analysis of Electric Machinery and Drive Systems. Piscataway, NJ: Wiley-IEEE Press, 2013.

[48] A. E. Samani, J. D. M. De Kooning, N. Kayedpour, N. Singh, and L. Vandevelde, "The Impact of Pitch-To-Stall and Pitch-To-Feather Control on the Structural Loads and the Pitch Mechanism of a Wind Turbine," Energies, vol. 13, no. 17, p. 4503, Sep. 2020, doi: 10.3390/en13174503.

[49] Gurobi Optimization, LLC. "Gurobi Optimizer Reference Manual," 2023. [Online]. Available: https://www.gurobi.com

[50] "Datasets", Energinet, 2021. [Online]. Available: https://www.energidataservice.dk/search. [Accessed: 05- Oct- 2023].

[51] "ENTSO-E Transparency Platform", Transparency.entsoe.eu, 2021. [Online]. Available: https://transparency.entsoe.eu/. [Accessed: 05- Oct- 2023].

JEROEN D. M. DE KOONING (Senior Member, IEEE) was born in Kapellen, Belgium, in 1987. He received the Master of Science and Ph.D. degrees in electromechanical engineering from Ghent University, Belgium, in 2010 and 2015 respectively. Since 2019, he is assistant professor at the Department of Electromechanical, Systems and Metal Engineering at the Faculty of Engineering and Architecture of Ghent University, Belgium. In 2022, he was a visiting professor at the Lappeenranta University Of Technology, Finland. He conducted research on current waveform shaping techniques for permanent magnet synchronous machines, and optimal control and design of renewable energy systems. His present research interests include modelling, optimization and control of mechatronic systems, drivetrains and manufacturing machines in an Industry 4.0 context, with a particular interest in digital twins. He is a member of the Dynamical Systems and Control (DySC) research group, the FlandersMake@UGent MIRO core lab and a senior member of the IEEE.

FRANÇOIS VALLÉE received the degree in civil electrical engineering and the Ph.D. degree in electrical engineering from the Faculty of Engineering, University of Mons, Belgium, in 2003 and 2009, respectively. He is currently a Professor and leader of the "Power Systems and Markets Research Group" at the University of Mons. His Ph.D. work has been awarded by the SRBE/KBVE Robert Sinave Award in 2010. His research interests include PV and wind generation modeling for electrical system reliability studies in presence of dispersed generation.

NARENDER SINGH received his Masters of science degree in electric power engineering from KTH Royal Institute of Technology, Sweden in 2015. He joined the Department of Electromechanical, Systems and Metal Engineering at the Faculty of Engineering and Architecture of Ghent University, Belgium in 2019 and received the Ph.D degree in 2023. His research interests include renewable energy and power systems studies.

LIEVEN VANDEVELDE (M '05, SM '07) was born in Eeklo, Belgium in 1968. He graduated in electrical & mechanical engineering (main subject: electrical power engineering) at Ghent University in 1992 and is since then with the Electrical Energy Laboratory (EELAB), Department of Electromechanical, Systems and Metal Engineering, Ghent University. He received the Ph.D. degree from Ghent University in 1997, and has conducted research in various domains of electrical power engineering, *inter alia* electrical machines and (computational) electromagnetics. Since 2004, he has been member of the professorial staff and has been coordinating the research on electric power systems at EELAB. In this research, renewable energy and its integration in electric power systems play a prominent role. He is member of EnerGhentIC, the interdisciplinary community of Ghent University researchers working on the energy challenge.

SEYYED AHMAD HOSSEINI received the Ph.D. degree in electrical engineering from the Power Systems and Markets Research Group, University of Mons, Mons, Belgium, in 2023. He is currently a Postdoctoral Researcher in the same group. Furthermore, he was an Adjunct Research Fellow at Federation University, Australia, in the first quarter of 2023. His research interests include machine learning, integration of wind power into electricity markets, and decision-making under uncertainty.

⚫ ⚫ ⚫